buildings

MDPI

Article

Thermo-Mechanical Coupling Model for Energy Piles: Dynamic Interface Behavior and Sustainable Design Implications

Chunyu Cui [1], Zhongren Liu [2], Jinghang Liu [3] and Yang You [1,*]

[1] Shandong Key Laboratory of Technologies and Systems for Intelligent Construction Equipment, Shandong Jiaotong University, Jinan 250357, China; 230007@sdjtu.edu.cn
[2] Shandong Luqiao Group Co., Ltd., Jinan 250014, China; was2415@163.com
[3] Institute of Geotechnical and Underground Engineering, Shandong University, Jinan 250061, China; sduljh@mail.sdu.edu.cn
* Correspondence: 220122@sdjtu.edu.cn

Abstract

This study introduces an advanced temperature variation model for the pile–soil interface of single energy piles, developed through extensive numerical simulations across diverse operating conditions. Unlike existing models, it explicitly accounts for thermal interactions at the interface by adopting uniform material properties and initial temperatures, enabling precise heat transfer predictions. An iterative algorithm based on the load transfer method quantifies the pile's thermo-mechanical response to temperature fluctuations, demonstrating significantly improved accuracy in settlement prediction compared to conventional methods. Validation against two field case studies demonstrates the model's robustness across varied geotechnical contexts. Parameter analysis identifies soil thermal conductivity and load transfer characteristics as critical factors influencing pile behavior, thereby facilitating design optimization. This approach enhances energy pile efficiency by up to 20%, promoting the utilization of renewable geothermal energy and reducing carbon emissions in infrastructure projects, thus contributing to sustainable geotechnical engineering practices.

Keywords: energy piles; pile-soil interface; thermomechanical response; numerical modeling; sustainable infrastructure

check for updates

Academic Editor: Bingxiang Yuan

Received: 27 August 2025
Revised: 24 October 2025
Accepted: 28 October 2025
Published: 4 November 2025

Citation: Cui, C.; Liu, Z.; Liu, J.; You, Y. Thermo-Mechanical Coupling Model for Energy Piles: Dynamic Interface Behavior and Sustainable Design Implications. *Buildings* **2025**, *15*, 3984. https://doi.org/10.3390/buildings15213984

Copyright: © 2025 by the authors. Licensee MDPI, Basel, Switzerland. This article is an open access article distributed under the terms and conditions of the Creative Commons Attribution (CC BY) license (https://creativecommons.org/licenses/by/4.0/).

1. Introduction

Shallow geothermal energy offers a sustainable and renewable solution for reducing energy consumption in buildings, with energy piles emerging as a dual-purpose technology for structural support and heat exchange [1]. Compared to conventional geothermal systems such as boreholes or buried tubes, energy piles provide superior cost-effectiveness and thermal efficiency [2–6]. The complex thermomechanical coupling involved in geothermal systems, akin to that analyzed in wellbore studies [7], necessitates advanced modeling approaches for energy piles. However, temperature-induced thermal stresses pose significant challenges, often surpassing structural loads and complicating practical applications [8,9].

To mitigate these issues, the load transfer method has been widely adopted to analyze the thermomechanical behavior of single energy piles under cyclic thermal loads [2,10,11]. While effective for individual piles, this approach struggles to capture the complex thermal interactions at the pile–soil interface, particularly under varying geotechnical conditions. Various load-transfer models, including the ideal elastoplastic [12], exponential [13], and hyperbolic models [14], have been successfully applied in conventional pile analysis,

providing valuable references for modeling energy pile behavior. Moreover, existing studies largely overlook the collective response of energy pile groups, leaving a gap in understanding interface-specific temperature effects [15–19].

This study addresses these limitations by proposing an advanced temperature variation model for single energy piles, developed through comprehensive numerical simulations. The model uniquely integrates unit skin friction, relative displacement, and end resistance at the pile–soil interface, offering improved predictions of heat transfer and mechanical response. An iterative algorithm, grounded in the load transfer method, quantifies the pile's reaction to temperature fluctuations, validated against recent field cases [15–19]. A parameter analysis further elucidates the influence of soil properties and load transfer on thermomechanical performance.

2. Temperature Variation Model of Pile–Soil Interface of Single Energy Pile

2.1. Introduction of Numerical Model of Pile–Soil Interface

Heat exchange between an energy pile and its surrounding soil is a complex process governed by thermal and mechanical interactions at the pile–soil interface. To model temperature variations effectively, this study employs a refined numerical approach, building on previous work [17] by explicitly capturing interface-specific heat transfer dynamics. The model is based on the following assumptions: (1) the pile and soil are homogeneous and isotropic, simplifying thermal field calculations; (2) both are thermoelastic bodies, consistent with linear deformation theory; (3) material properties (e.g., elastic modulus, thermal expansion coefficient) are temperature-independent, a common approximation for small temperature ranges; (4) the pile, soil, and heat exchange tube share an initial temperature of 22 °C, with boundary soil temperature held constant; (5) operating conditions reflect seasonal extremes—summer room temperature at 38 °C and tube fluid at 35 °C, winter room temperature at 0 °C and tube fluid at 4 °C; (6) the radial dimension of the heat exchanger is neglected in the tubeline flow model to focus on axial heat transfer. These assumptions, while idealized, align with standard geotechnical modeling practices [17] and are assessed for sensitivity in Section 4.

The energy pile, depicted in Figure 1a, has a diameter of 1.6 m and a burial depth of 20 m, constructed from reinforced concrete and embedded in sandy soil. A single U-shaped steel heat exchange tube, with an inner diameter of 30 mm, wall thickness of 3 mm, and burial depth of 14.5 m, facilitates heat transfer using water as the circulating fluid. A one-dimensional linear heat transfer model governs fluid-tube wall interactions, while the solid domain is discretized with tetrahedral finite elements, as shown in Figure 1b. A denser mesh is applied near the pile to resolve high thermal gradients, ensuring numerical accuracy. Material properties for sand and concrete are sourced from Gao et al. [17], with water as the heat exchange fluid (Table 1). Simulations were conducted using COMSOL5.6, enhancing precision over traditional analytical methods.

Table 1. Material parameters.

Material	Density [kg/m^3]	Constant Pressure Heat Capacity [J/(kg·K)]	Thermal Conductivity [W/(m·K)]
Water (exchange fluid)	1000	4200	0.62
Sandy soil (soil around pile)	1730	1200	1.68
Concrete (energy pile)	2500	960	1.92
Heat exchange tube	7870	440	50.0

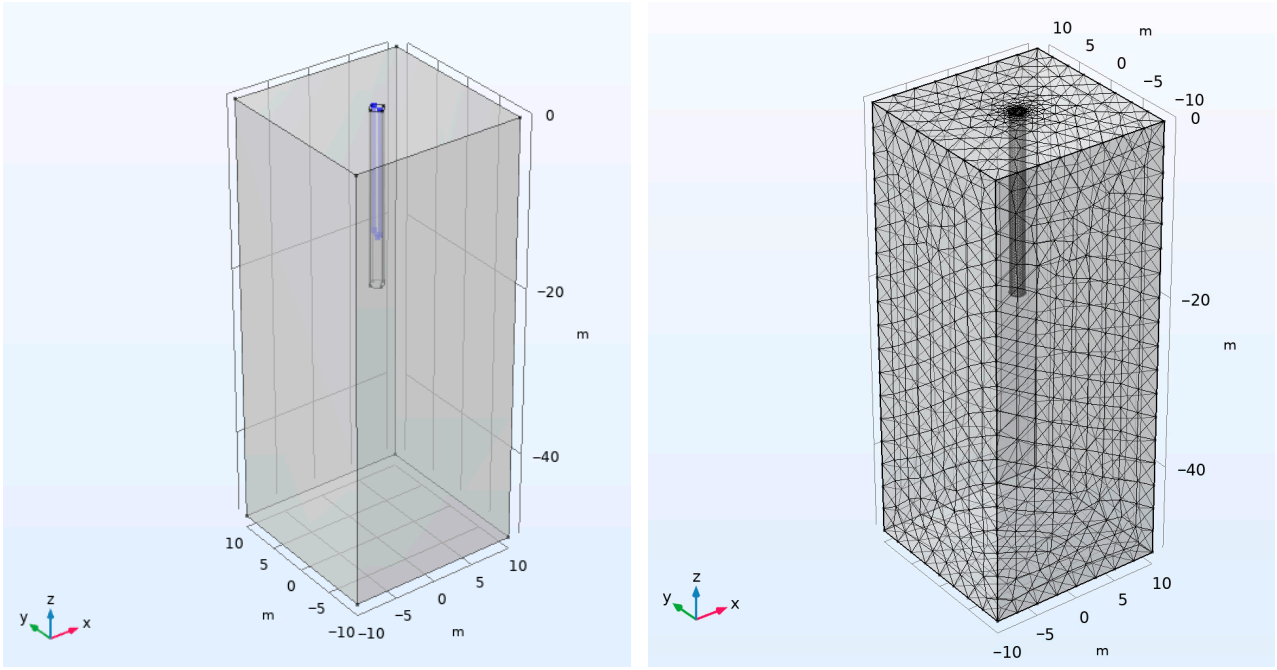


Figure 1. Schematic diagram of pile–soil interface of energy pile model: (**a**) overall model; and (**b**) grid division of the model.

2.2. Boundary Conditions and Mesh Design

The dimensions of the computational domain were selected to ensure that all boundaries are far enough from the heat source to remain unaffected by its thermal influence. Specifically, the radial extent was set to 3–4 times the pile diameter, as simulations and previous work [20] show that temperature changes beyond this distance are insignificant. This setup guarantees that the boundaries act as a constant-temperature condition, set to the initial ground temperature. At the initial state (t = 0), a uniform temperature of 22 °C was prescribed for the entire system, including the heat exchange tube, the energy pile, and the surrounding soil, i.e.:

$$T_c(x,\ y,\ z,\ 0) = 22\ ^\circ\mathrm{C} \tag{1}$$

The lateral and bottom boundaries of the model are defined as constant-temperature boundaries, maintaining the initial temperature throughout the analysis:

$$T_c(x,\ t) = T_c(y,\ t) = 22\ ^\circ\mathrm{C} \tag{2}$$

The top of the energy pile, which interfaces with the superstructure, is assumed to be exposed to the ambient air. Diurnal temperature fluctuations are neglected, and constant temperatures representing seasonal extremes are applied—38 °C for summer and 0 °C for winter conditions:

$$\begin{cases} T_c(x,\ y,\ 0,\ t) = 0\ ^\circ\mathrm{C} & \text{winter} \\ T_c(x,\ y,\ 0,\ t) = 38\ ^\circ\mathrm{C} & \text{summer} \end{cases} \tag{3}$$

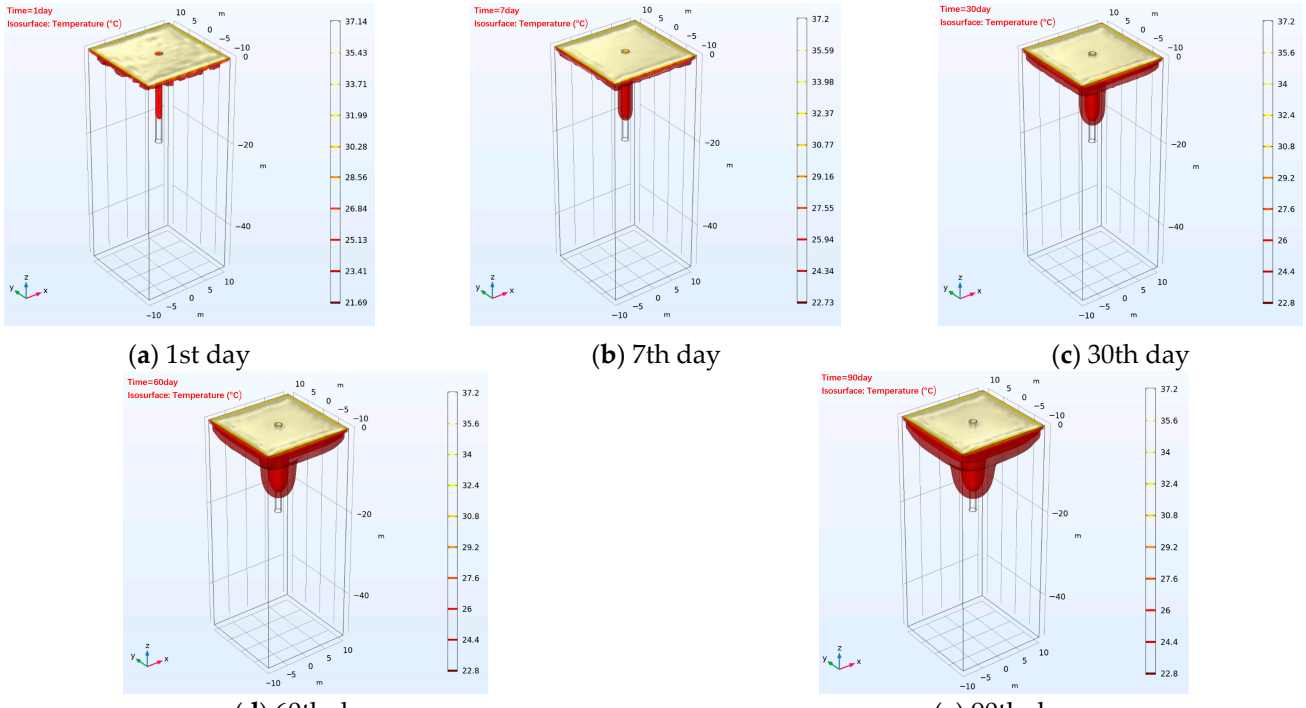
The solid domains of the model were discretized using tetrahedral elements. A refined mesh was applied to the energy pile and the adjacent soil, where the most intensive heat exchange occurs, to ensure accuracy in capturing high thermal gradients. A coarser mesh was utilized for the outer soil regions to achieve an optimal balance between computational efficiency and solution precision. The resulting mesh of the model is illustrated in Figure 1b.

It should be noted that the model assumes a constant seasonal temperature at the ground surface, neglecting diurnal temperature fluctuations and solar radiation. This is because the significant influence of such transient disturbances is typically confined to shallow soil layers [6]. For a 20-meter-deep energy pile, its primary mechanical behavior is dominantly controlled by the deep soil temperature field driven by the heat exchange tube. This simplification helps to focus on the core processes of interest in this study, and the good agreement between the model and measured data (see Section 5) demonstrates its validity.

2.3. Results Analysis

The transient numerical model simulates daily temperature variations in the energy pile and surrounding soil over a 90-day period. Heat transfer is driven by temperature gradients between the fluid in the heat exchange tube, the pile, and the soil. In summer, elevated external temperatures increase the fluid temperature, leading to heat transfer from the fluid to the pile and subsequently to the soil. Conversely, in winter, the fluid absorbs heat from the pile and soil, thereby increasing its own temperature while decreasing that of the pile and soil.

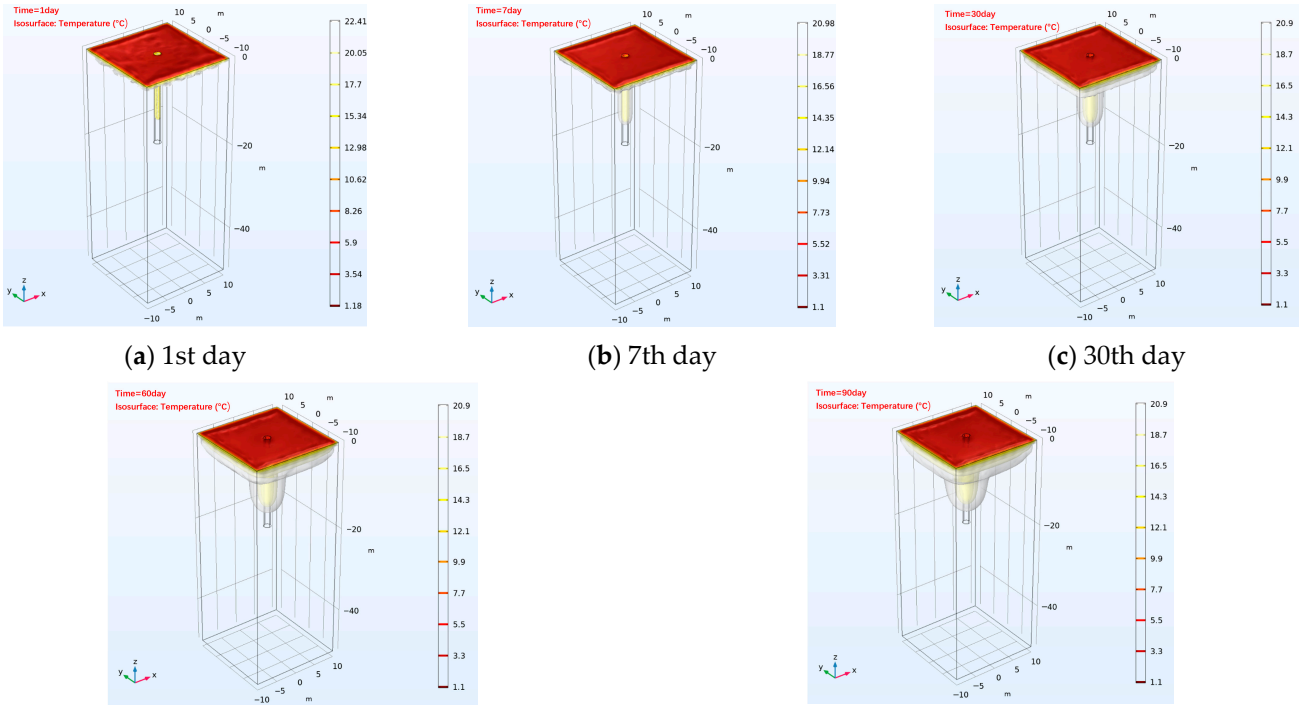
Figures 2 and 3 depict isotherms illustrating the temperature distributions in the pile and soil on the 1st, 7th, 30th, 60th, and 90th days for both summer and winter conditions. The isotherms reveal a progressive stabilization of heat transfer between the energy pile and the surrounding soil. Initially, a significant temperature gradient between the heat exchange tube and the pile results in rapid internal heat transfer. After approximately 7 days, the dominant heat transfer mechanism shifts to external diffusion into the surrounding soil. By the 60th day, thermal equilibrium is nearly achieved, with minimal further changes in temperature distribution.



(**a**) 1st day (**b**) 7th day (**c**) 30th day

(**d**) 60th day (**e**) 90th day

Figure 2. Isotherm surface in summer.



(**a**) 1st day (**b**) 7th day (**c**) 30th day

(**d**) 60th day (**e**) 90th day

Figure 3. Isotherm surface in winter.

Despite seasonal variations, the fundamental heat exchange mechanism remains consistent, governed by soil thermal properties and the temperature differential between the fluid and soil. For identical soil conditions, the temperature difference is set at 5 °C for both seasons, though the absolute temperature disparity is greater in winter due to lower ambient conditions. Consequently, the spatial extent of temperature influence (i.e., the thermal diffusion range) is larger in winter under equivalent simulation parameters.

Upon reaching thermal stability (approximately day 60), the temperature distribution in the surrounding soil is examined along the y-axis at various depths. Specifically, cross-sectional temperature profiles are extracted along the y–z plane (x = 0) at depths z = 14.5 m, z = 10 m, and z = 5 m, corresponding to the bottom of the heat exchange tube, mid-depth, and near-surface, respectively. These profiles, presented in Figures 4 and 5 for summer and winter, respectively, illustrate the vertical variation in soil temperature during the stable phase.

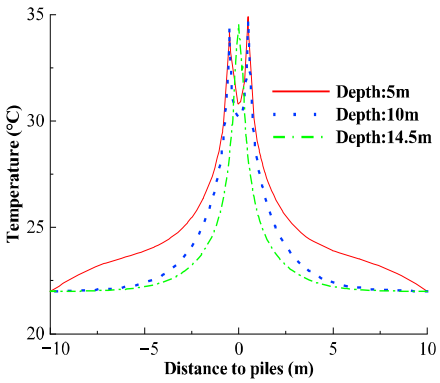


Figure 4. Summer temperature.

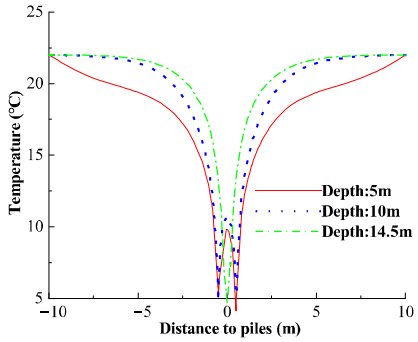


Figure 5. Winter temperature.

Figures 4 and 5 demonstrate that at a depth of 5 m, the soil temperature surrounding the energy pile exhibits greater variability due to the influence of surface ambient conditions, in contrast to the relatively stable temperatures observed at 10 m and 14.5 m. This variability stems from the model's assumption of constant ambient temperatures (0 °C in winter and 38 °C in summer), which overlooks real-world factors such as diurnal temperature fluctuations and solar radiation. As a result, the simulated heat transfer extends deeper than would occur under actual conditions, where surface heat loss mitigates temperature diffusion. Furthermore, the enhanced heat transfer observed at z = 14.5 m, compared to z = 5 m and z = 10 m, is attributed to the U-shaped heat exchange tube's bottom being located at z = 14.5 m, acting as a concentrated heat source.

Figure 6 depicts the temperature profile at the pile–soil interface, showing a stable temperature from the surface to approximately 14.5 m, consistent with the uniform heat source provided by the fluid within the heat exchange tube. Beyond 14.5 m, the temperature drops sharply due to a reduced temperature gradient between the pile and the surrounding soil, leading to diminished heat transfer rates. This pattern aligns with the temperature model proposed by Liu et al. [21], which divides the pile–soil interface into two distinct zones: (1) from the top of the pile to the depth of the heat exchange tube (z = 14.5 m), where the interface temperature matches that of the exchange fluid; and (2) from the tube's depth to the pile's base, where the temperature exhibits an exponential decay, as described by Equation (4).

$$T_{pc} = T_0 + \frac{T_f - T_0}{e^z - e^{H_b}} e^{H_0} + \frac{T_0 e^z - T_f e^{H_b}}{e^z - e^{H_b}} \quad (4)$$

where T_{pc} denotes the temperature at the pile–soil interface, T_0 is the initial temperature at the interface, T_f is the fluid temperature within the heat exchange tube of the energy pile, H_z is the depth at the point of interest, H_b is the total embedded depth of the energy pile, and H_0 is the installation depth of the heat exchange tube.

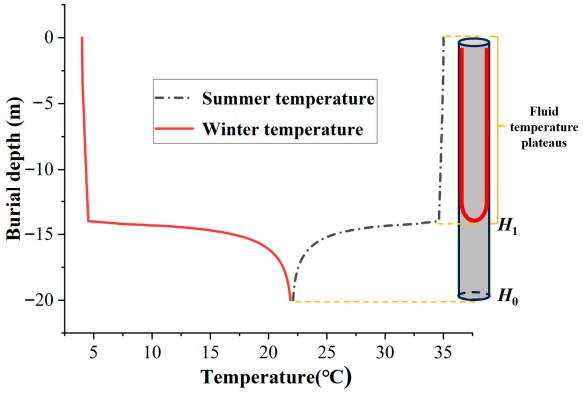


Figure 6. Temperature profile at the pile–soil interface.

3. Analytical Solution for the Temperature Field of Soil Surrounding Energy Piles

3.1. Heat Transfer Model of Energy Piles

This section develops an analytical model for the temperature field in the soil surrounding an energy pile, employing a finite-length solid cylindrical heat source model. This approach provides precise temperature predictions without requiring detailed modeling of internal heat transfer within the pile, and it demonstrates good agreement with established line and helical heat source models in terms of thermal power output.

The analytical solution is based on the following assumptions:

(1) The surrounding soil is homogeneous, isotropic, and possesses temperature-independent thermal properties; (2) Groundwater flow is neglected; (3) The soil domain is sufficiently large such that boundary temperatures remain unaffected by the energy pile; (4) The initial soil temperature is uniformly set to 0 °C; (5) Only temperature variations induced by the energy pile, treated as a single heat source, are considered, with surface temperature effects disregarded.

As depicted in Figure 7, the heat transfer model for the energy pile and surrounding soil is formulated using Green's function. This involves solving for an instantaneous point heat source and integrating the solution over both time and space to capture the transient thermal response.

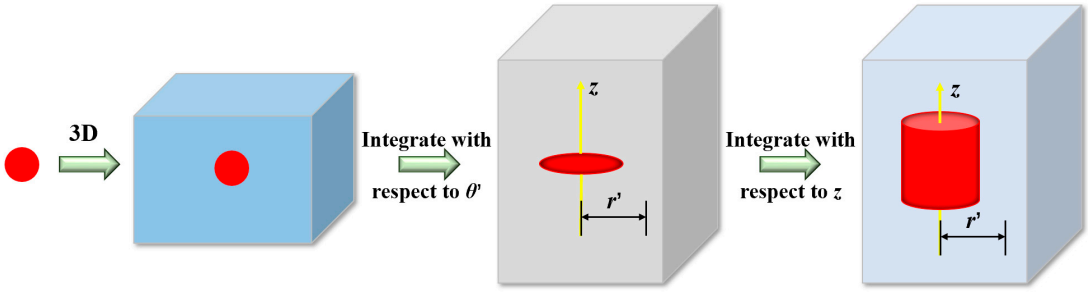


Figure 7. Heat source relationship of a finite length solid cylinder.

A solid cylindrical heat source can be conceptualized as an assembly of numerous ring-shaped heat sources distributed along its height. To formulate the instantaneous ring-shaped heat source model, we treat it as the integration of instantaneous point heat source models over a ring of radius r' at time t'. In cylindrical coordinates, assuming the heat generation of the ring source is $q\mathrm{d}r'\mathrm{d}z'$, the instantaneous ring-shaped heat source model is derived by integrating the point heat source model over the angular coordinate θ'. This integration yields the following expression:

$$\Delta T = \frac{q}{2\pi\rho c}\int_0^t \mathrm{d}t\prime \int_0^{2\pi} G(r,\theta,z,t;r\prime,\theta\prime,z\prime,t\prime)\mathrm{d}\theta\prime \tag{5}$$

where $G(r, \theta, z, t, r'; \theta', z', t')$ is the Green's function, representing the temperature response to a unit point heat source. By integrating Equation (5), we obtain:

$$\Delta T = \frac{q}{8\rho c}\int_0^t \frac{1}{\sqrt{(\pi a_v(t-t\prime)^3}} I_0\left(\frac{rr\prime}{2a_v(t-t\prime)}\right)\exp\left(-\frac{r^2+r\prime^2+(z-z\prime)^2}{4a_v(t-t\prime)}\right)\mathrm{d}t\prime \tag{6}$$

where $I_0(x)$ is the zero-order modified Bessel function, and q is the heat generation intensity of the heat source. The equation for solving q is:

$$q = a_v\prime c_p m_p \Delta T \cdot (1 + k\nabla T_{\text{pile}}) \tag{7}$$

where $a_v{}'$ is the heat transfer coefficient at the pile–soil interface, c_p is the specific heat capacity of the energy pile, m_p is the mass of the energy pile, ΔT is the temperature change in the energy pile, ∇T_{pile} is the correction factor for the temperature gradient inside the pile (optional, default is 0). The energy pile can be modeled as a collection of multiple ring-shaped heat sources distributed along its height. For simplified analysis, it is usually assumed that the temperature at the pile–soil interface is approximately equal to the average temperature inside the pile; if internal heat transfer within the pile needs to be considered, it can be adjusted through the correction factor ∇T_{pile}.

The energy pile can be modeled as an assemblage of infinitely ring-shaped heat sources distributed along its height. The heat transfer model for the surrounding soil is derived by integrating the thermal response of these ring-shaped heat sources, each treated as a line heat source, along the vertical axis of the pile. To precisely account for boundary conditions, the method of images is employed in the solution process [22]. The resulting heat transfer equation is given by:

$$\Delta T = \frac{q}{8\rho c}\int_0^{H_b} \mathrm{d}z\prime \int_0^t \frac{1}{\sqrt{(\pi a_v(t-t\prime))^3}} \tag{8}$$

$$I_0\left(\frac{rr\prime}{2a_v(t-t\prime)}\right)\left[\exp\left(-\frac{r^2+r\prime^2+(z-z\prime)^2}{4a_v(t-t\prime)}\right)-\exp\left(-\frac{r^2+r\prime^2-(z+z\prime)^2}{4a_v(t-t\prime)}\right)\right]\mathrm{d}t\prime \tag{9}$$

The temperature at the pile–soil interface of an energy pile reaches stabilization within approximately 7 days. In the analytical solution for the temperature field, heat transfer within the pile is neglected, and the interface temperature is assumed to equal the internal temperature of the energy pile. The embedded portion of the heat exchange tube within the pile is modeled as a cylindrical heat source with a uniform temperature, corresponding to the fluid temperature inside the tube. For depths below the installation depth of the heat exchange tube, the interface temperature is determined using Equation (4). To model the temperature variation along the energy pile, the embedded heat exchanger is divided into two segments at depth H_0: above H_0, the heat source is treated as constant with a uniform temperature equal to that of the fluid; below H_0 to the pile base, it is treated as a variable temperature heat source. The resulting temperature profile of the energy pile is illustrated in Figure 8 and mathematically expressed by Equation (10).

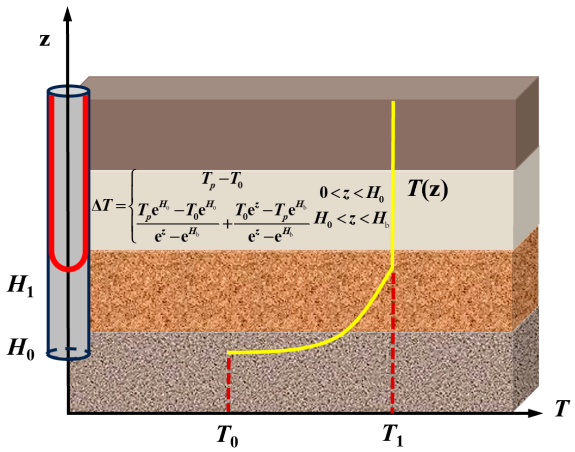


Figure 8. Schematic diagram of temperature variation model at the pile–soil interface.

3.2. Limitations of the Heat Transfer Model of Energy Piles

The analytical heat transfer model proposed in this study is based on the assumptions of a homogeneous, isotropic porous medium without groundwater flow. These simplifications may introduce certain biases in the predictions. First, neglecting groundwater advection underestimates the effective thermal diffusivity of the soil. In permeable strata (e.g., sand or gravel), groundwater flow can significantly enhance heat transport, potentially increasing the effective thermal conductivity by a factor of 1.5 to 3 compared to conduction alone [23]. Consequently, the present model may overestimate the magnitude of temperature changes in the soil surrounding the pile (e.g., the actual temperature increase/decrease in an active flow field could be 20–50% lower than predicted) and prolong the predicted time to reach thermal equilibrium. Second, the model assumes constant material thermal properties. In reality, parameters such as soil thermal conductivity vary with temperature, an effect more pronounced with changing water content. For the typical operating temperature range of energy piles (~0 °C to ~40 °C), the bias introduced by this dependency is generally less than 10% [24], but becomes critical when phase change (e.g., freeze-thaw) or a larger temperature span is involved. While the conclusions drawn under these simplified assumptions in this study, which focuses on revealing the core thermo-mechanical mechanism at the pile–soil interface, remain of significant theoretical value, the incorporation of a convective-diffusive heat transfer equation and temperature-dependent material properties is recommended for sites with significant groundwater flow or when high-precision long-term thermal power prediction is required.

$$\Delta T = \begin{cases} T_p - T_{0,} & 0 < z < H_0 \\ \frac{T_p e^{H_0} - T_0 e^{H_0}}{e^z - e^{H_b}} + \frac{T_0 e^z - T_p e^{H_b}}{e^z - e^{H_b}} & , H_0 < z < H_b \end{cases} \tag{10}$$

Combined with Equation (4), the heat source intensity q can be obtained as:

$$q = \begin{cases} a\prime_v c_p m_p \left(\frac{T_p - T_0}{e^z - e^{H_b}} e^{H_0} + \frac{T_0 e^z - T_f e^{H_b}}{e^z - e^{H_b}} \right), H_0 < z < H_b \\ a\prime_v c_p m_p \left(T_p - T_0 \right), 0 < z < H_0 \end{cases} \tag{11}$$

In practical engineering, the embedded depth of the heat exchange tube within the energy pile is significantly less than the total depth of the energy pile. Therefore, when calculating the temperature variation in the surrounding soil, the temperature change from the embedded depth of the heat exchange tube to the bottom of the pile can be neglected. Consequently, the energy pile can be approximated as a uniform cylindrical heat source, simplifying the expression for the heat intensity q'. Based on the previously defined heat source intensity q, the modified q' can be expressed as:

$$q\prime = a\prime_v c_p m_p \left(T_p - T_0 \right) \tag{12}$$

By applying Equation (10), the equation describing the temperature variation in the soil surrounding the energy pile is derived as follows:

$$\Delta TQ = \frac{q\prime}{8\rho c} \int_0^t \frac{1}{\sqrt{(\pi a_v (t - t'))^3}} I_0 \left(\frac{rr\prime}{2a_v (t - t\prime)} \right) \int_0^{H_b} \left[\exp\left(-\frac{r^2 + r'^2 + (z - z\prime)^2}{4a_v (t - t\prime)} \right) - \exp\left(-\frac{r^2 + r\prime^2 + (z + z\prime)^2}{4a_v (t - t\prime)} \right) \right] \mathrm{d}z\prime \mathrm{d}t\prime \tag{13}$$

4. Calculation of Settlement for a Single Energy Pile

Calculating the settlement of energy piles requires accounting for thermal stresses induced by temperature changes. Wu et al. [25] demonstrated that temperature cycling in energy piles, under the constraints of overlying loads and surrounding soil, leads to additional stresses and irreversible settlements. Hence, it is essential to incorporate temperature effects into settlement analyses.

In this section, the load transfer method is utilized to calculate the settlement of energy piles, given its proven capability in describing pile foundation behavior. During operation, energy piles undergo heat exchange with the surrounding soil, leading to temperature fluctuations. However, the heat transfer model presented earlier does not account for these transient temperature variations. Therefore, settlement is calculated under the assumption of stable heat exchange conditions, with the transient temperature phase neglected.

For the load transfer model, an exponential function is adopted for the shaft friction, while a hyperbolic function is used for the base resistance. The hyperbolic form is chosen for the pile tip as it simplifies parameter estimation and more accurately captures its mechanical behavior.

4.1. Control Equation for a Single Energy Pile

The load transfer method discretizes the energy pile into n elastic segments, each interacting with the surrounding soil through nonlinear load transfer functions that represent the soil's resistance along the shaft. The pile tip is modeled using either a linear or nonlinear spring to simulate end-bearing resistance, as depicted in Figure 9. The model relies on the following assumptions: (1) both the energy pile and the surrounding soil are homogeneous and isotropic; (2) both materials exhibit thermoelastic behavior with constant thermal properties; (3) temperature effects at the pile tip are neglected, assuming negligible heat transfer or thermal stress at the base; (4) the energy pile is treated as a solid cylindrical heat source; and (5) thermal deformation is considered in the axial (z-direction) and radial directions, with axial deformation assumed to be independent of the surrounding soil's constraints.

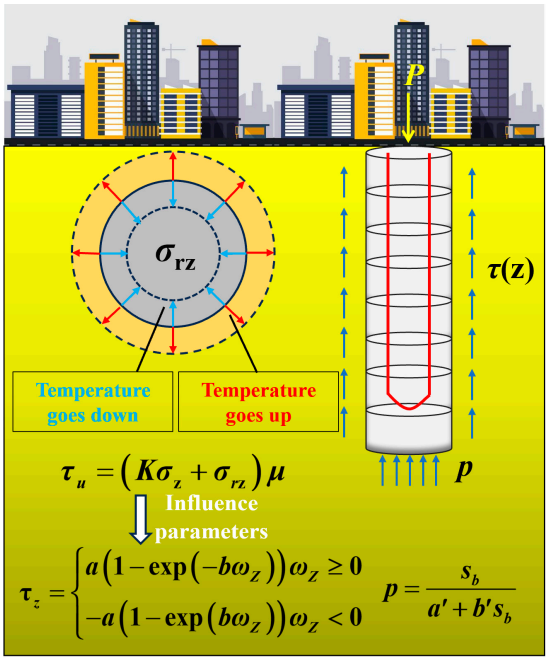


Figure 9. Schematic diagram of load transfer method.

The displacement $S(z)$ at depth z along the pile can be represented as:

$$S(z) = s_t - \int_0^z \frac{P(z)}{E_p A_p} \mathrm{d}z \tag{14}$$

The axial force $P(z)$ at depth z along the pile can be represented as:

$$P(z) = P_t - \pi d \int_0^z \tau_s(z) \mathrm{d}z \tag{15}$$

where s_t represents the displacement at the pile top, P_t is the load at the pile top, E_p is the elastic modulus of the pile, A_p is the cross-sectional area of the pile, d is the diameter of the pile, and $\tau_s(z)$is the lateral friction resistance along the pile.

By differentiating Equation (14) with respect to z and taking the second derivative of Equation (15) with respect to z, and then combining the two, the load transfer differential equation that relates the lateral friction resistance $\tau_s(z)$ and the pile displacement $S(z)$ at depth z for the energy pile is obtained as:

$$\frac{\pi \mathrm{d}\tau(z)}{E_p A_p} = \frac{\mathrm{d}^2 S(z)}{\mathrm{d}z^2} \tag{16}$$

The load transfer differential equation for energy piles is structurally similar to that of ordinary piles, with differences arising in the boundary conditions and parameter selection. In energy piles, these parameters are affected by temperature changes. By solving the differential equation, the axial force, settlement, and lateral friction resistance at various points of the energy pile can be determined.

4.2. Establishment of the Mechanical Model for the Pile Side

In the analysis of energy piles, the displacement of the pile at depth z is assumed to consist of two components: (1) the elastic displacement of the surrounding soil; (2) the relative displacement at the pile–soil interface.

The thermal expansion and contraction of the pile, induced by temperature changes, are incorporated into the relative displacement at the pile–soil interface. To accurately describe the relationship between the pile shaft shear stress and the relative displacement at the pile–soil interface ω_z, an exponential function model is employed, which can be expressed as:

$$\tau_z = \begin{cases} a(1 - \exp(-b\omega_Z)), \omega_Z \geq 0 \\ -a(1 - \exp(b\omega_Z)), \omega_Z < 0 \end{cases} \tag{17}$$

where τ_z represents pile shaft shear stress, and a and b are model parameters. Figure 10 outlines the calibration pathway for parameters a and b.

The elastic displacement of the soil surrounding the energy pile, influenced by temperature changes, will be slightly enhanced but remains relatively small and linearly elastic. This can be estimated using the shear displacement method proposed by Randolph and Wroth [26]. The expression for the shear displacement method is as follows:

The elastic displacement of the soil surrounding the energy pile, influenced by temperature changes, experiences a minor increase but remains within the linear elastic range. This displacement can be estimated using the elastic continuum method proposed by Randolph and Wroth [26]. The formula for displacement is given by:

$$\omega_s = \frac{r_0}{G_0} \ln\left(\frac{r_m}{r_0}\right) \tau_z \tag{18}$$

where r_0 is the pile radius, G_0 is the shear modulus of the surrounding soil, r_m is radius of influence around the pile shaft which can be calculated by Equation (19).

$$r_m = 2.5\rho(1 - v_s)L \tag{19}$$

where v_s is the Poisson's ratio of the surrounding soil, ρ is the non-uniformity coefficient of the surrounding soil, given by $\rho = G_{savg}/G_L$, G_L is the average shear modulus and G_{savg} is the shear modulus at depth L. For homogeneous soil, $\rho = 1$.

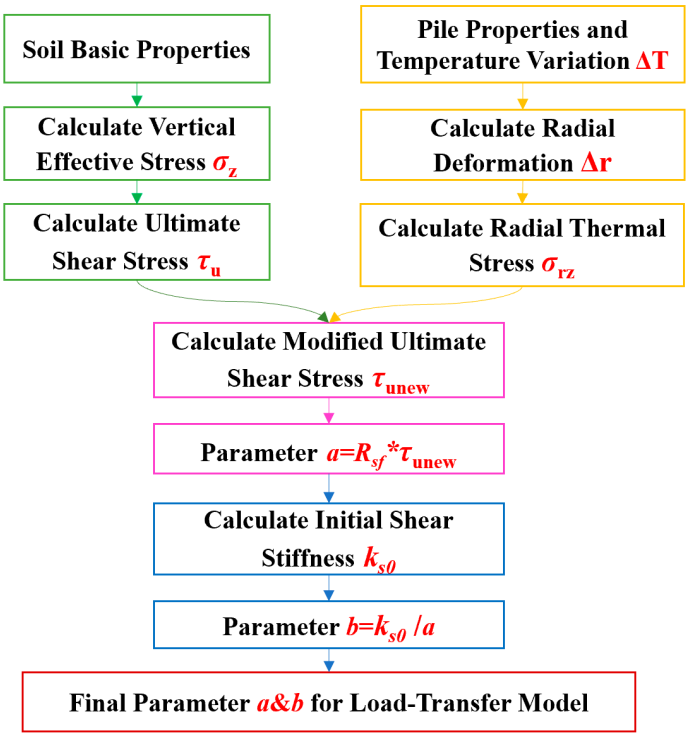


Figure 10. Calibration pathway for parameters a and b.

The differential control equation for energy piles, along with the load transfer curves for pile shaft friction and pile displacement, has been fully established. To solve this equation, the model parameters a and b in the mechanical model for the pile shaft must be determined.

In this mechanical model, a and b are parameters influenced by temperature variations in energy piles. In the load transfer model for conventional pile foundations, which uses an exponential function, a represents the pile–soil interface failure shear stress, while b is the ratio of the initial shear stiffness to the failure shear stress. For energy piles specifically, these parameters can be expressed as:

$$a = \tau_f \tag{20}$$

$$b = \frac{k_{s0}}{\tau_f} \tag{21}$$

where k_{s0} represents the initial shear stiffness at the pile–soil interface of a pile foundation, τ_f represents the failure shear stress at the pile–soil interface of the energy pile.

The failure shear stress τ_f at the pile–soil interface of a pile foundation can be expressed as:

$$\tau_f = R_{sf}\tau_u \tag{22}$$

where R_{sf} represents the pile shaft shear failure ratio, generally ranging from 0.80 to 0.95; τ_u is the ultimate shear stress at the pile shaft, generally obtained by Equation (20).

$$\tau_u = K\sigma_z \tan\varphi \tag{23}$$

where σ_z is the vertical effective stress at depth z, ρ is the soil density, g is the acceleration due to gravity, z is the depth of the soil, K is the lateral earth pressure coefficient, which is recommended to be the coefficient of earth pressure at rest K_0, and can be calculated using the formula: $K_0 = 1 - \sin(\varphi)$, φ is the angle of internal friction of the soil.

The initial shear stiffness of the pile–soil interface k_{s0}, according to the empirical formula proposed by Randolph and Wroth [26], is defined by the expression:

$$k_{s0} = \frac{G_0}{r_0 \ln\left(\frac{r_m}{r_0}\right)} \tag{24}$$

During the operation of an energy pile, temperature changes induce additional effective stress at the pile–soil interface. When the energy pile heats up, both the pile and the surrounding soil expand, increasing the vertical effective stress at depth z. Conversely, cooling causes the pile and the surrounding soil to contract, reducing the vertical effective stress at depth z, as shown in Figure 9.

The shear strength at the pile–soil interface is defined as the product of the ultimate shear stress τ_u and the pile shaft shear failure ratio R_{sf}. The ultimate shear stress at the pile–soil interface, denoted as τ_{unew}, accounts for both the self-weight stress of the surrounding soil and the additional stress induced by temperature changes, and is expressed as:

$$\tau_{unew} = (K\sigma_z + \sigma_{rz})\mu \tag{25}$$

where μ is the friction coefficient at the pile–soil interface; σ_{rz} is the thermal stress generated by temperature changes in the energy pile.

The radial thermal stress induced by temperature changes in the energy pile σ_{rz} can be determined using the method proposed by Liu [27], which builds on the cavity expansion analysis method developed by Faizal et al. [28]. The expression for the radial thermal stress in the energy pile σ_{rz} is given by:

$$\sigma_{rz} = \frac{\Delta r E_s}{(1 + \upsilon_s) r_0} \tag{26}$$

where E_s is the elastic modulus of the surrounding soil, Δr is the radial deformation of the energy pile under temperature changes, ν_s is the Poisson's ratio of the surrounding soil, r_0 is the initial radius of the pile.

To determine the radial deformation Δr of the energy pile under temperature changes, it is assumed that the axial deformation of the energy pile, due to temperature effects, is linearly elastic. The volumetric thermal expansion coefficient of the energy pile is three times the linear thermal expansion coefficient ($3\alpha = \beta$; α: the linear thermal expansion coefficient; β: the volumetric thermal expansion coefficient). Using the deformation compatibility condition, the calculation method for the radial deformation Δr of the energy pile under temperature influence is derived. The detailed process is as follows:

Based on the assumptions, the deformation in the z-direction due to temperature changes in the energy pile can be expressed as:

$$\Delta z = L_T - L_0 = \alpha \Delta T L_0 \tag{27}$$

where L_0 represents the initial length of the energy pile, L_T represents the length of the energy pile after temperature changes, ΔT represents the change in temperature, Δz represents the deformation in the z-direction.

The volume change in the energy pile due to temperature variations is given by:

$$\Delta V = V_T - V_0 = \beta \Delta T V_0 \tag{28}$$

where V_0 represents the initial volume of the energy pile, V_T represents the volume of the energy pile after temperature changes, ΔV represents the change in volume.

Substituting the volume formula for a cylinder into Equation (28) yields the expression:

$$r_T^2 L_T = (1 + 3\alpha) r_0^2 L_0 \tag{29}$$

where r_T represents the radius of the energy pile after temperature changes.

Combining Equation (27), the expression for the radial deformation of the energy pile under temperature influence Δr is given by:

$$\Delta r = r_0 \left(\sqrt{\frac{1 + 3a\Delta T}{1 + a\Delta T}} - 1 \right) \tag{30}$$

By substituting Equation (30) into Equation (27), the expression for the radial thermal stress in an energy pile σ_{rz} is derived as follows:

$$\sigma_{rz} = \frac{\Delta r E_s}{(1 + v_s) r_0} = \frac{\left(\sqrt{\frac{1+3a\Delta T}{1+a\Delta T}} - 1 \right) E_s}{(1 + v_s)} \tag{31}$$

The expression for the ultimate shear stress at the energy pile–soil interface, accounts for both the self-weight stress of the surrounding soil and the additional stress induced by temperature changes is given by Equation (32).

$$\tau_{unew} = (K\sigma_z + \sigma_{rz})\mu = \left(K\sigma_z + \frac{\left(\sqrt{\frac{1+3a\Delta T}{1+a\Delta T}} - 1 \right) E_s}{(1 + v_s)} \right) \mu \tag{32}$$

The temperature variation in the energy pile is given by Equation (10).

4.3. Establishment of the Mechanical Model for the Pile End

Studies on the mechanical behavior of energy pile tips reveal that temperature cycles induce plastic strain in the soil at the pile tip, resulting in a progressive increase in soil pressure [29]. However, the effect of temperature cycles on the compressive stress at the pile tip is relatively small and stabilizes over time. As a result, the temperature effect at the pile tip is neglected in this analysis. To accurately model the pressure-displacement behavior at the pile tip, a widely adopted hyperbolic model is employed as the mechanical model for the pile tip. The hyperbolic model is expressed as:

$$p = \frac{s_b}{a\prime + b\prime s_b} \tag{33}$$

where p denotes the pile tip resistance, S_b represents the pile tip displacement; a' and b' are the model parameters.

In the pile-end model, the parameters are defined in terms of the initial stiffness of the soil at the pile end, as given by Equation (34):

$$a\prime = \frac{1}{k_{sb}} \tag{34}$$

where the initial stiffness of the soil at the pile end k_{sb} can be determined based on the research by Randolph and Wroth [26]:

$$k_{sb} = \frac{4G_b}{\pi r_0(1-v_b)} \tag{35}$$

where G_b is the shear modulus and v_b is the Poisson's ratio of the soil at the pile end.

The model parameter b' can be represented as follows:

$$b\prime = \frac{R_b}{p_{bu}} \tag{36}$$

where R_b represents the shear stress ratio at pile end failure, typically ranging from 0.75–0.8; and p_{bu} denotes the ultimate bearing capacity per unit area of the soil at the pile end.

Based on the cavity expansion theory proposed by Vesic [30], the ultimate bearing capacity per unit area at the pile end can be expressed as:

$$p_{bu} = cN_c + \overline{p}N_p \tag{37}$$

where c represents the cohesion of the load-bearing soil layer, $\overline{p}$ represents the average vertical pressure on the lateral surface of the pile tip, N_c and N_p are the dimensionless bearing capacity factors corresponding to the cohesive force c and the self-weight of the sliding soil mass below the pile base, respectively.

The bearing capacity factor N_c is given by:

$$N_c = (N_p - 1)\cot\varphi \tag{38}$$

where φ represents the internal friction angle of the load-bearing soil layer.

The average vertical pressure on the lateral surface of the pile tip, denoted as $\overline{p}$, is given by:

$$\overline{p} = \frac{1+2K_0}{3}\gamma h \tag{39}$$

where K_0 represents the coefficient of static earth pressure of the soil, γ denotes the effective unit weight of the soil above the pile tip plane, and h denotes the depth of the pile.

The bearing capacity factor N_p, which depends on the failure surface mode of the soil at the pile tip, can be categorized into two forms. The first form corresponds to Vesic's pile tip failure mode, as illustrated in Figure 11, and is given by:

$$N_{pV} = \tan^2\left(\frac{\pi}{4}+\frac{\varphi}{2}\right) I_{rr}\frac{3}{3-\sin\varphi}\exp\left[\left(\frac{\pi}{2}-\varphi\right)\tan\varphi\right]\frac{4\sin\varphi}{3(1-\sin\varphi)} \tag{40}$$

where I_{rr} represents the stiffness correction factor.

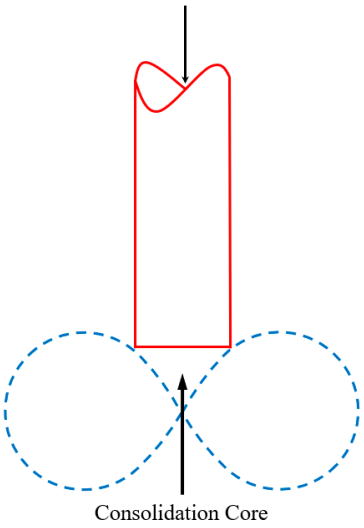


Figure 11. Vesic pile tip soil failure mode.

The second form corresponds to the Janbu's pile tip failure mode as illustrated in Figure 12, and is given by:

$$N_{pJ} = \left(\tan\varphi + \sqrt{1+\tan^2\varphi}\right)^2 \exp(2\psi\tan\varphi) \tag{41}$$

where ψ is the angle between the pile tip consolidation boundary and the horizontal plane, with values typically ranging from 60° to 105° depending on the compressibility of the soil.

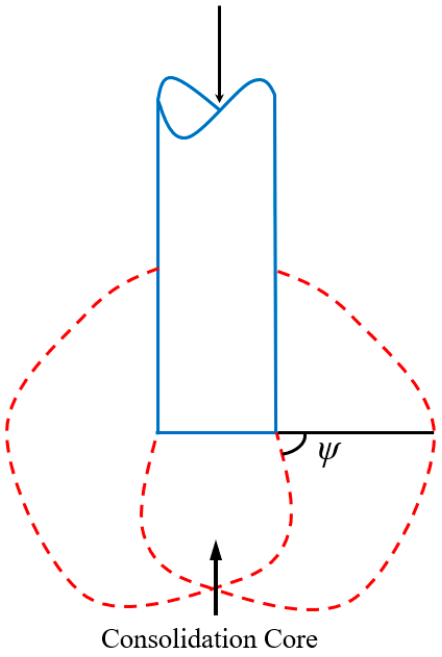


Figure 12. Janbu pile tip soil failure mode.

4.4. Settlement Calculation Procedure for a Single Energy Pile

This study adopts the deformation coordination method to determine the load-settlement relationship of a single energy pile. The procedure is outlined as follows:

1. Discretize the pile into n segments and assign node numbers from 0 to n, with the pile tip node designated as $n + 1$.
2. Apply a pile top load Q and initially estimate the displacements of two pile nodes, $S1\ z$ and $S2\ z$, setting them to minimal values.
3. Compute the shaft friction $\tau 1\ z$ and $\tau 2\ z$ for these nodes using the pile shaft load transfer model.
4. Assuming linear variation in the axial force within the pile segment, the elastic compression S_c of segment 1 is given by:

$$S_c = \frac{Q + \left(Q - \pi dl \frac{\tau_z^1 + \tau_z^2}{2}\right)}{2} \left(\frac{\Delta l}{E_p A_p}\right) \tag{42}$$

5. Adjust the displacement at node 2 as:

$$S_z^2\prime = S_z^1 - S_c \tag{43}$$

6. Compare the adjusted displacement $S2'\ z$ with the initially assumed displacement $S2\ z$. If the absolute difference is less than 1×10^{-6}, adopt $S2'\ z$ as the displacement at node 2; otherwise, repeat steps 3–5 until the difference is less than 1×10^{-6}.
7. Calculate the displacements for the remaining pile nodes.
8. Using the node displacements calculate the pile shaft friction for each pile segment and sum them to obtain the total pile shaft friction Q_z.
9. Using the pile tip load transfer model and the calculated displacement of the pile tip node $Sn\ z$, determine the pile tip load Q_b.
10. Calculate the total bearing capacity of the pile Q':

$$Q\prime = Q_z + Q_b \tag{44}$$

11. Vary the pile top load Q and repeat steps 2–10 to generate a series of pile top displacements and their corresponding loads, establishing the load-settlement relationship.

5. Validation of Single Energy Pile Model

5.1. Case Study 1: Friction-Type Energy Pile in Kunshan, China

Jiang et al. [31] investigated the behavior of a friction-type energy pile in Kunshan, China, by developing a numerical model for a 40-meter-long energy pile. Their study focused on the bearing characteristics under thermo-mechanical coupling effects, analyzing the variations in bearing capacity and pile top displacement due to temperature changes. Specifically, the energy pile's temperature increased by 20 °C under summer conditions and decreased by 15 °C under winter conditions. The pile was equipped with U-shaped polyethylene (PE) heat exchange tubes, embedded to a depth of 39 m. The thermal and physical properties of the energy pile and the surrounding soil are provided in Tables 2 and 3, respectively.

Table 2. Thermal and physical properties of energy piles.

Pile Length (m)	Pile Diameter (m)	Elastic Modulus (GPa)	Density (kg/m^3)	Poisson's Ratio	Coefficient of Thermal Expansion (m/°C)
40	0.6	30	2500	0.2	1×10^{-5}

Table 3. Thermal and physical properties of soil around the energy pile.

Number	Soil Layer	Thickness (m)	Density (kg/m^3)	Internal Friction Angle (°)	Elastic Modulus (MPa)	Pile–Soil Friction Coefficient	Poisson's Ration	Cohesion (kPa)
1	Plain fill	3.0	1800	11.6	28	0.2	0.35	9
2	Topsoil	2.0	1800	11.6	28	0.2	0.35	9
3	Silty clay	1.5	1830	12.8	25	0.2	0.35	22
4	Silty clay with silt	2.0	1830	10.0	15	0.2	0.40	13
5	Silty clay	5.0	1940	15.0	80	0.2	0.35	42
6	Silt with fine sand	6.0	1840	25.1	100	0.3	0.30	8
7	Fine Sand with silt	6.0	1860	27.1	140	0.3	0.30	6
8	Silt	2.5	1810	22.1	120	0.3	0.30	9
9	Silt	12.0	1840	25.2	200	0.3	0.30	8

The load-settlement relationship for the energy pile was computed using the method proposed in this study, incorporating the numerical model parameters provided by Jiang et al. [31]. The results obtained from our method were compared with those from Jiang et al.'s numerical model, as shown in Figure 13. The close agreement between the outcomes of our load-settlement calculation method and Jiang et al.'s [31] numerical model demonstrates that our approach effectively captures the load-settlement behavior of energy piles under both heating and cooling conditions.

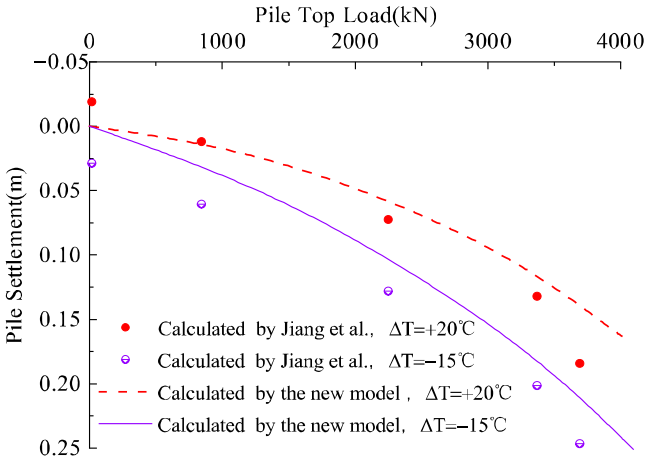


Figure 13. Comparison diagram of load-settlement curve of energy pile in case study 1 [31].

5.2. Case Study 2: PHC Energy Piles at Henan Zhoukou Normal College Sports Complex, China

Ren et al. [32], supported by the Henan Zhoukou Normal College Sports Complex project in China, conducted field experiments to investigate the thermodynamic characteristics and load-bearing performance of prestressed high-strength concrete (PHC) energy piles. Their findings indicated that temperature variations significantly influenced the axial forces within the energy piles, leading to an uneven distribution along the pile depth and inducing negative skin friction along the pile shaft. The experiments utilized PHC tubular piles with a length of 12 m, a diameter of 0.4 m, and a wall thickness of 95 mm. The tests were conducted over 120 h, encompassing three distinct thermal conditions achieved by varying the fluid flow rates in the heat exchange tubes. During the load-settlement tests, the initial temperature of the energy pile was 18 °C, which increased by 13 °C over the course of the experiments. The detailed thermal and physical properties of the energy pile and the surrounding soil are provided in Tables 4 and 5, respectively.

Table 4. Thermal property parameters of energy piles.

Pile Length (m)	Pile Diameter (m)	Elastic Modulus (GPa)	PHC Tube Wall Thickness (m)	Poisson's Ratio	Coefficient of Thermal Expansion (m/°C)
12	0.4	38	0.95	0.2	1×10^{-5}

Table 5. Thermal property parameters of soil around energy pile.

Number	Soil Layer	Thickness (m)	Density (kg/m^3)	Internal Friction Angle (°)	Elastic Modulus (MPa)	Pile–Soil Friction Coefficient
1	Mixed fill soil	1.1	19.3	20.8	8.24	0.5
2	Silt	1.4	19.8	18.6	9.88	0.5
3	Silty clay	1.8	17.9	9.7	5.33	0.5
4	Silt	1.4	19.4	7.4	3.50	0.5
5	Silty clay	3.5	18.2	10.8	5.85	0.5
6	Silty clay	1.5	18.6	15.8	8.42	0.5
7	Silty sand	1.4	19.3	13.2	18.00	0.5

In the vicinity of the energy piles, the soil primarily consists of silt and silty clay, with the Poisson's ratio of each soil layer assumed to be 0.3. The load-settlement curves of the energy piles, derived using the method proposed in this study, were compared with results from on-site model tests conducted by Ren et al. [32], as shown in Figure 14. The close agreement between the load-settlement curves obtained from our method and those from Ren et al.'s [32] field tests, as observed in Figure 14, demonstrates that the proposed load-settlement calculation method effectively and accurately captures the load-settlement behavior of energy piles under temperature variations.

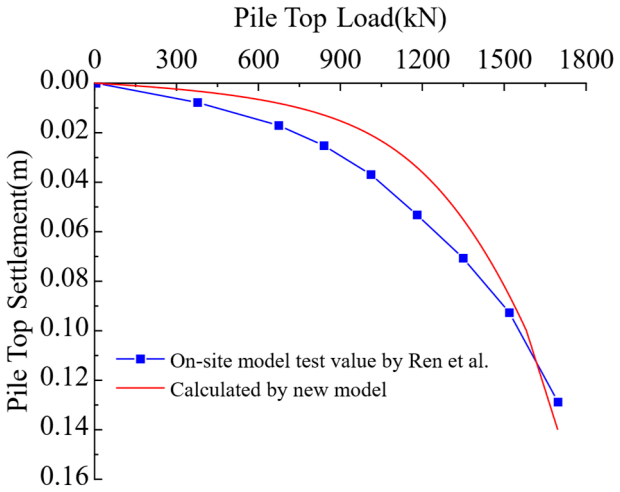


Figure 14. Comparison diagram of load-settlement curve of energy pile in case study 2 [32].

6. Conclusions and Future Work

This study has developed a comprehensive thermo-mechanical model for single energy piles through integrated numerical simulations and analytical modeling. The proposed framework accurately captures the temperature variation at the pile–soil interface and its consequent effects on the pile's load-settlement behavior under thermal loading. Validation

against field case studies demonstrates the model's reliability as a robust tool for energy pile design across diverse geotechnical conditions.

From a design perspective, this research provides substantial support for sustainable infrastructure development. The methodology presented herein, through its improved settlement prediction accuracy, enables more optimized and confident design of energy pile systems. These systems offer significant advantages by serving dual structural and energy functions: they effectively utilize shallow geothermal energy through fluid circulation in embedded pipes, exchanging heat between buildings and the ground. This integration eliminates the need for dedicated boreholes, enhancing both cost-effectiveness and thermal efficiency compared to conventional geothermal systems.

The environmental benefits are substantial—by displacing fossil fuel consumption for building heating and cooling, energy piles significantly reduce carbon emissions and air pollutants while aligning with sustainable development goals. Operated with minimal electricity for circulation pumps, these systems provide efficient space heating in winter by extracting ground heat, and cooling in summer by rejecting building heat to the ground.

While this study establishes a solid foundation for single energy pile analysis, it also identifies several promising research directions for enhanced predictive capabilities. Future work will focus on developing a more sophisticated cyclic thermo-mechanical coupling framework incorporating: (1) transient thermal boundary conditions including diurnal fluctuations and groundwater flow effects; (2) temperature-dependent material properties, particularly for soil thermal conductivity and pile–soil interface friction; (3) advanced constitutive models capturing interface ratcheting and soil stiffness degradation under cyclic loading; (4) temperature-dependent pile-tip mechanical behavior; and (5) extension to energy pile clusters accounting for thermal interaction effects. Validating such an advanced framework will require comprehensive experimental data, including laboratory testing of soil-concrete interface behavior under thermal cycles, field monitoring of pile-tip thermomechanical response, and systematic measurements of thermal property variations across different soil types.

This work contributes to the growing body of knowledge supporting the integration of geothermal technology into foundation systems, promoting wider adoption of energy piles as a key element in sustainable urban development and the transition to renewable energy sources.

Author Contributions: Conceptualization, C.C. and Y.Y.; methodology, J.L.; software, Z.L.; validation, C.C., Z.L. and J.L.; formal analysis, C.C.; investigation, Z.L.; resources, C.C. and Y.Y.; data curation, C.C.; writing—original draft preparation, Z.L.; writing—review and editing, C.C.; visualization, Z.L.; supervision, Y.Y.; project administration, J.L.; funding acquisition, C.C. and Y.Y. All authors have read and agreed to the published version of the manuscript.

Funding: This research was funded by project ZR2023QE324, ZR2024ME215 and ZR2024QE474 by Shandong Provincial Natural Science Foundation.

Institutional Review Board Statement: Not applicable.

Informed Consent Statement: Not applicable.

Data Availability Statement: The data that support the findings of this study are available from the corresponding author upon reasonable request.

Acknowledgments: The authors also extend their sincere appreciation to the editors and anonymous reviewers for their constructive comments and suggestions, which have significantly improved the quality of this manuscript.

Conflicts of Interest: Author Zhongren Liu was employed by Shandong Luqiao Group Co., Ltd. The remaining authors declare that the research was conducted in the absence of any commercial or financial relationships that could be construed as a potential conflict of interest.

Abbreviations

The following abbreviations are used in this manuscript:

T_{pc}	temperature at the pile–soil interface;
ΔT	temperature variation in the energy pile;
q	intensity of the heat source;
q'	modified intensity of the heat source;
ΔT_Q	temperature variation in the soil surrounding the energy pile;
$S(z)$	displacement at depth z along the pile;
$P(z)$	axial force at depth z along the pile;
τ_z	pile shaft shear stress;
ω_s	relative displacement between the energy pile and the soil;
r_m	radius of influence around the pile shaft;
a	pile–soil interface failure shear stress;
b	ratio of the initial shear stiffness to the failure shear stress;
τ_f	failure shear stress;
τ_u	ultimate shear stress at the pile shaft;
k_{s0}	initial shear stiffness of the pile–soil interface;
τ_{unew}	ultimate shear stress at the pile–soil interface, accounts for both the self-weight stress of the surrounding soil and the additional stress induced by temperature changes;
σ_{rz}	radial thermal stress induced by temperature changes in the energy pile;
Δz	deformation in the z-direction due to temperature changes in the energy pile;
ΔV	volume change in the energy pile due to temperature variations;
Δr	radial deformation of the energy pile under temperature influence;
p	the pile tip resistance;
a'	model parameter;
b'	model parameter;
k_{sb}	initial stiffness of the soil at the pile end;
p_{bu}	ultimate bearing capacity per unit area of the soil at the pile end;
N_c	bearing capacity factor;
$\overline{p}$	average vertical pressure on the lateral surface of the pile tip;
N_{pV}	bearing capacity factor corresponds to Vesic's pile tip failure mode;
N_{pJ}	bearing capacity factor corresponds to Janbu pile tip failure mode
S_c	the elastic compression;
Q'	total bearing capacity of the pil.

References

1. Ding, X.; Peng, C.; Wang, C.; Kong, G. Heat transfer performance of energy piles in seasonally frozen soil areas. *Renew. Energy* **2022**, *190*, 903–918. [CrossRef]
2. Park, S.; Lee, D.; Choi, H.J.; Jung, K.; Choi, H. Relative constructability and thermal performance of cast-in-place concrete energy pile: Coil-type GHEX (ground heat exchanger). *Energy* **2015**, *81*, 56–66. [CrossRef]
3. Zarrella, A.; De Carli, M.; Galgaro, A. Thermal performance of two types of energy foundation pile: Helical tube and triple U-tube. *Appl. Therm. Eng.* **2013**, *61*, 301–310. [CrossRef]
4. Murphy, K.; Gao, J.; Olgun, C.G. Performance and sustainability of energy piles. *Renew. Sustain. Energy Rev.* **2014**, *35*, 1–12.
5. Hamada, Y.; Hirose, S.; Nakamura, H. Long-term performance of energy piles in different climatic conditions. *Geothermics* **2021**, *89*, 101882.
6. Laloui, L.; Loria, A.F.R. Thermo-mechanical analysis of energy piles: A review of critical aspects and challenges. *Geomech. Energy Environ.* **2019**, *19*, 100127.
7. Fan, Z.; Parashar, R. Analytical solutions for a wellbore subjected to a non-isothermal fluid flux: Implications for optimizing injection rates, fracture reactivation, and EGS hydraulic stimulation. *Rock Mech. Rock Eng.* **2019**, *52*, 4715–4729. [CrossRef]

8. Suryatriyastuti, M.; McCartney, J.S.; Stewart, M.A. Thermal and mechanical behavior of energy piles in unsaturated silt. *J. Geotech. Geoenviron. Eng.* **2012**, *138*, 1069–1082.
9. Zhang, B.; Wang, J.; Wang, R. Analytical solutions for the thermo-mechanical behavior of energy piles. *Renew. Energy* **2018**, *116*, 196–208.
10. Di Donna, A.; Ferrari, A.; Laloui, L. Experimental investigations of the soil-concrete interface: Physical mechanisms, cyclic mobilisation and behaviour at different temperatures. *Can. Geotech. J.* **2016**, *53*, 659–672. [CrossRef]
11. Loria, A.F.R.; Laloui, L. Group action effects caused by various operating energy piles. *Géotechnique* **2018**, *68*, 834–841. [CrossRef]
12. Sarkar, P.; Pant, P. Nanavati Physical phenomena during nanoindentation deformation of amorphous glassy polymers. *Polymer* **2024**, *312*, 295–307. [CrossRef]
13. Wang, S.D.; Du, H.; Wei, G.; Peng, P.; Xuan, P. Experimental modification of the internal solitary wave force exerted on a horizontal transverse cylinder due to wave-flow and vortex shedding. *Ocean Eng.* **2023**, *269*, 113513. [CrossRef]
14. Kim, B.T.; Kim, N.K.; Lee, W.J.; Kim, Y.S. Experimental load-transfer curves of laterally loaded piles in Nak-Dong River sand. *J. Geotech. Geoenviron. Eng.* **2004**, *130*, 416–425.
15. Behbehani, F.; McCartney, J.S. Energy pile groups for thermal energy storage in unsaturated soils. *Appl. Therm. Eng.* **2022**, *215*, 119028. [CrossRef]
16. Stewart, M.A.; McCartney, J.S. Strain distributions in centrifuge model energy foundations. In Proceedings of the GeoCongress 2012: State of the Art and Practice in Geotechnical Engineering, Oakland, CA, USA, 25–29 March 2012; pp. 4376–4385.
17. Gao, J.; Zhang, R.; Liu, J.; Li, K.; Yang, J. Numerical and experimental assessment of thermal performance of vertical energy piles: An application. *Appl. Energy* **2008**, *85*, 901–910. [CrossRef]
18. Köhler, J.; Jäschke, M.; Weber, M. Thermal performance of energy piles in different climates. *Renew. Energy* **2017**, *114*, 160–172.
19. Di Donna, A.; Laloui, L. Advancements in geotechnical design of energy piles. In Proceedings of the International Workshop on Geomechanics and Energy—The Ground as Energy Source and Storage, Lausanne, Switzerland, 26–28 November 2013; pp. 26–28.
20. Liu, J.; Zhang, Q.; Xiao, K.; Cui, W.; Liu, Z. Study on the thermo-mechanical response of a single energy pile in pile groups. *Structures* **2025**, *71*, 108013. [CrossRef]
21. Liu, S.; Zhang, Q.; Liu, J.; Cui, W.; Yu, X. A simple method for predicting the response of single energy pile considering temperature variation of pile-soil interface. *Int. J. Geomech.* **2023**, *23*, 04022293. [CrossRef]
22. Li, Q.; Zheng, M.; Qiao, L.; Sui, Z. Transient heat transfer model of a three-dimensional spiral heat source in an energy pile. *Chin. J. Eng.* **2021**, *43*, 1569–1576.
23. Chiasson, A.; O'Connell, A. New analytical solution for sizing vertical borehole ground heat exchangers in environments with significant groundwater flow: Parameter estimation from thermal response test data. *HVACR Res.* **2011**, *17*, 1000–1011. [CrossRef]
24. Côté, J.; Konrad, J.M. A generalized thermal conductivity model for soils and construction materials. *Can. Geotech. J.* **2005**, *42*, 443–458. [CrossRef]
25. Wu, D.; Liu, H.; Kong, G.; Wang, C.; Che, P. Study on bearing characteristics of energy piles with embedded and tied buried tubes. *Acta Energiae Solaris Sin.* **2017**, *38*, 1109–1116. (In Chinese)
26. Randolph, M.F.; Wroth, C.P. Analysis of vertical deformation of vertically loaded piles. *Int. J. Rock Mech. Min. Sci. Geomech. Abstr.* **1978**, *104*, 1465–1488.
27. Liu, J.H. Study on Bearing Characteristics of Energy Piles Considering Temperature Variation Effects at the Pile-Soil Interface. Master's Thesis, Shandong University, Jinan, China, June 2022. (In Chinese).
28. Faizal, M.; Bouazza, A.; Haberfield, C.; McCartney, J.S. Axial and radial thermal responses of a field-scale energy pile under monotonic and cyclic temperature changes. *J. Geotech. Geoenviron. Eng.* **2018**, *144*, 04018072. [CrossRef]
29. Chang, H.; Zhu, W.; Wang, Y.; Gu, F. Mechanical characteristics of energy piles under temperature load. *Chin. Sci. Pap.* **2022**, *17*, 660–666. (In Chinese)
30. Vesic, A.S. Analysis of ultimate loads of soil mechanics and foundations. *J. Soil Mech. Found. Eng.* **1973**, *99*, 45–73. [CrossRef]
31. Jiang, G.; Li, R.; Wang, H.; Chen, G.; Lu, H.; Shao, D. Analysis of the thermal-mechanical coupling performance of friction-type energy piles. *Chinses J. Rock Mech. Eng.* **2019**, *38*, 2525–2534. (In Chinese)
32. Ren, L.; Ren, J.; Kong, G.; Liu, H. Field tests on thermal response and bearing performance of PHC energy piles under cyclic heating and cooling. *Rock Soil Mech.* **2021**, *42*, 529–536+546. (In Chinese)

Disclaimer/Publisher's Note: The statements, opinions and data contained in all publications are solely those of the individual author(s) and contributor(s) and not of MDPI and/or the editor(s). MDPI and/or the editor(s) disclaim responsibility for any injury to people or property resulting from any ideas, methods, instructions or products referred to in the content.